



3D Multi-Echo Dixon technique for simultaneous assessment of liver steatosis and iron overload in patients with chronic liver diseases: a feasibility study

Fubi Hu^{1,2}, Ru Yang¹, Zixing Huang², Min Wang², Fang Yuan², Chunchao Xia², Yi Wei², Bin Song²

¹Department of Radiology, The First Affiliated Hospital of Chengdu Medical College, Chengdu 610041, China; ²Department of Radiology, West China Hospital, Sichuan University, Chengdu 610041, China

Correspondence to: Dr. Bin Song. Department of Radiology, West China Hospital, Sichuan University, No. 37 Guoxue Alley, Wuhou District, Chengdu 610041, China. Email: Songlab_radiology@163.com.

Background: Patients with chronic liver diseases (CLDs) often suffer from lipidosis or siderosis. Proton density fat fraction (PDFF) and $R2^*$ can be used as quantitative parameters to assess the fat/iron content of the liver. The aim of this study was to evaluate the influence of liver fibrosis and inflammation on the 3D Multi-echo Dixon (3D ME Dixon) parameters (MRI-PDFF and $R2^*$) in patients with CLDs and to determine the feasibility of 3D ME Dixon technique for the simultaneous assessment of liver steatosis and iron overload using histopathologic findings as the reference standard.

Methods: Ninety-nine consecutive patients with CLDs underwent T1-independent, T2*-corrected 3D ME Dixon sequence with reconstruction using multipeak spectral modeling on a 3T MR scanner. Liver specimen was reviewed in all cases, grading liver steatosis, siderosis, fibrosis, and inflammation. Spearman correlation analysis was performed to determine the relationship between 3D ME Dixon parameters (MRI-PDFF and $R2^*$) and histopathological and biochemical features [liver steatosis, iron overload, liver fibrosis, inflammation, alanine aminotransferase (ALT), aspartate aminotransferase (AST), total bilirubin (TBIL)]. Multiple regression analysis was applied to identify variables associated with 3D ME Dixon parameters. Receiver operating characteristic (ROC) analysis was performed to determine the diagnostic performance of these parameters to differentiate liver steatosis or iron overload.

Results: In multivariate analysis, only liver steatosis independently influenced PDFF values ($R^2=0.803$, $P<0.001$), liver iron overload and fibrosis influenced $R2^*$ values ($R^2=0.647$, $P<0.001$). The Spearman analyses showed that $R2^*$ values were moderately correlated with fibrosis stages ($r=0.542$, $P<0.001$) in the subgroup with the absence of iron overload. The area under the ROC curve of PDFF was 0.989 for the diagnosis of steatosis grade 1 or greater, and 0.986 for steatosis grade 2 or greater. The area under the ROC curve of $R2^*$ was 0.815 for identifying iron overload grade 1 or greater, and 0.876 for iron overload grade 2 or greater.

Conclusions: 3D Multi-Echo Dixon can be used to simultaneously evaluate liver steatosis and iron overload in patients with CLDs, especially for quantification of liver steatosis. However, liver $R2^*$ value may be affected by the liver fibrosis in the setting of CLDs with absence of iron overload.

Keywords: Magnetic resonance imaging; chronic liver disease (CLD); steatosis; iron overload

Submitted Dec 19, 2018. Accepted for publication May 16, 2019.

doi: 10.21037/qims.2019.05.20

View this article at: <http://dx.doi.org/10.21037/qims.2019.05.20>

Introduction

Chronic liver disease (CLD) is a major global-scale public health problem, which can be caused by a variety of underlying etiologies including mainly viral infections, nonalcoholic fatty liver disease (NAFLD), alcoholic fatty liver disease, primary sclerosing cholangitis, primary hemochromatosis, and autoimmune disease. Among them, NAFLD is becoming the most common cause of CLD, and the prevalence is rapidly increasing worldwide (1). Liver fat, iron, and combined overload are common pathological manifestations in many CLDs (2-4).

Liver fat and iron deposits are risk factors for hepatocyte injury, leading to progressive fibrosis, cirrhosis and related complications (5). Furthermore, the coexistence of fat and iron overload is more harmful than iron overload alone and may further accelerate the progression of liver damage and portends a worse prognosis (5,6). Therefore, detection and quantification of liver steatosis and iron deposition have important clinical significance, and early recognition is crucial to appropriate management and prevent progression.

Currently, liver biopsy is the standard of reference for the assessment of liver steatosis and iron overload. However, it has inherent limitations including sampling error, observer variability, possible complications, and high costs (7). Also, biopsy-based histopathological evaluations are a semiquantitative scoring system, but it is not a continuous scale. Therefore, a biopsy is inappropriate for screening, longitudinal monitoring, and epidemiologic research (8). Thus, the development of a noninvasive, accurate and reproducible technique for quantification of depositional liver diseases would be great clinical value.

Recently, conventional cross-sectional imaging techniques have been used for detection and quantification of liver steatosis or iron overload, including ultrasonography, computed tomography, and MR imaging. Although enabled to detect liver steatosis, US are unable to quantify liver fat content and detect iron overload accurately. CT may detect liver steatosis and iron overload by measurement of attenuation but is not sensitive or specific due to histopathological confounders such as edema, congestion, inflammation, and glycogen-storage (3,8,9). With recent advances in MR technology, several MRI-based approaches have been developed for liver fat (e.g., signal fat fraction using phase-encoding GRE or frequency-selective approach, PDFF using multi-echo chemical shift-encoded or magnetic resonance spectroscopy) and iron quantification (e.g., signal intensity ratio, T2/R2 relaxometry, T2*/R2*

relaxometry). The PDFF is now generally accepted as the standardized imaging biomarker of liver fat (5,10-12). Additionally, the correction of T2* decay by acquiring more echoes is necessary for accurate computation of MRI-PDFF. Thus, confounder-corrected multi-echo Dixon MR imaging provides an opportunity to quantify fat and iron simultaneously.

Several studies have demonstrated that PDFF derived from confounder-corrected multi-echo Dixon have high accuracy and reproducibility (10,13-16). Although promising, most studies mainly focus on the quantification of liver fat using confounder-corrected multi-echo Dixon MR imaging in patients with fatty liver disease. Currently, it is unclear whether the same T2* estimation/correction method used for fat quantification is also optimal for T2* quantification in patients with iron overload (5). Additionally, various pathologic changes, including liver steatosis, iron deposition, fibrosis, and inflammation, are frequently coexisted in CLDs (17). Although addressing technical confounders, the effect of histopathological confounders (e.g., liver fibrosis and inflammation) on quantitative parameters measurement of confounder-corrected 3D multi-echo Dixon (3D ME Dixon) in patients with a wide spectrum of CLD remains unclear. Therefore, the purpose of this study was to evaluate the influence of liver fibrosis and inflammation on the 3D ME Dixon parameters in patients with CLDs and to determine the feasibility of 3D ME Dixon technique for the simultaneous assessment of liver steatosis and iron overload by using histopathologic findings as to the reference standard.

Methods

Patients

This retrospective study was approved by the Institutional Review Board (IRB), and informed consent was waived. Between January 2015 and May 2017, 202 consecutive patients who were suspected or known of having CLDs or hepatocellular carcinoma clinically or at previously performed ultrasonography or computed tomography underwent liver MR examinations including 3D multi-echo VIBE Dixon sequence. One hundred and three patients were subsequently excluded for the following reasons: poor image quality (n=16); patients who did not performed histopathologic examinations (n=17) or unavailable histopathologic reports (n=12); previous partial hepatectomy or total splenectomy (n=11); patients underwent previous interventional therapy (n=16);

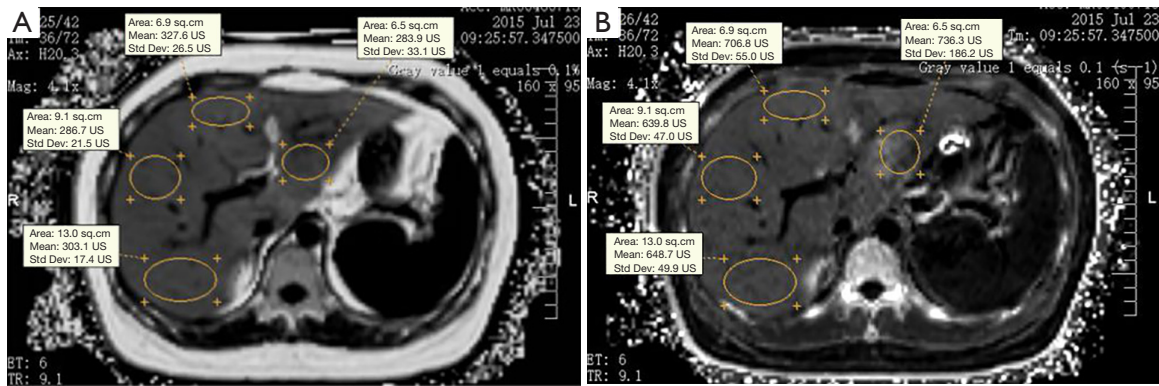


Figure 1 MRI-PDFF (A) and R2* (B) maps of a 45-year-old woman with NAFLD (liver steatosis grade 2, iron grade 1, fibrosis stage 2 and inflammation grade 1) determined by histologic validation. Four largest-fit ROIs (one per the right lobe anterior, right lobe posterior, left lobe medial, and left lobe lateral segment) were manually positioned in the homogeneous liver parenchyma at the level of the right main portal vein. MRI-PDFF and R2* values were directly derived by drawing ROI on the related parameter maps. NAFLD, nonalcoholic fatty liver disease; ROI, region of interest; PDFF, proton density fat fraction.

numerous or massive liver lesions ($n=31$). Finally, 99 patients were enrolled in this study, with a mean age of 48.39 ± 17 years (range, 23–77 years). Fifty-three men (mean age, 47.81 ± 15.5 years; range, 26–76 years) and 46 women (mean age, 49.07 ± 27 years; range, 23–77 years) were included.

MR examination

MRI examinations were performed on a 3.0 T system (MAGNETOM Skyra, Siemens AG, Erlangen, Germany) with 18 channels body phased-array coils. After routine coronal T2-weighted Half-Fourier acquisition single-shot turbo spin-echo (HASTE) sequence, axial breath-hold T2-weighted turbo spin-echo (TSE) sequence, axial T1-weighted dual-echo sequence and diffusion-weighted imaging (DWI), a 3D multi-echo VIBE Dixon sequence was obtained in all patients with the following parameters: 6 TEs of 1.05, 2.46, 3.69, 4.92, 6.15, and 7.38 ms, TR 9.15 ms, slice thickness 3.5 mm, flip angle of 4° to reduce the T1 effect, matrix size of 160×95 , and a field-of-view (FOV) 420×315 mm, bandwidth 1,040 Hz/Px. A parallel acceleration technique was employed, with acceleration factors of 2. Acquisition time was 16 s. A Levenberg-Marquardt nonlinear fitting was then used to fit the magnitude of the complex signal of the multiecho data. Inline reconstruction was performed by addressing confounders that included field inhomogeneity, eddy current, T1 bias, T2* decay and spectral complexity, and

MRI proton density fat fraction (PDFF) and R2* maps were automatically generated based on a pixel-by-pixel fitting.

Image analysis

Quantitative parameters measurement were independently performed by two radiologists who were blinded to clinical data and histopathological results. MRI-PDFF and R2* values were directly derived by drawing region of interest (ROI) on the related parameter maps. For each patient, four ROI (one per the right lobe anterior, right lobe posterior, left lobe medial, and left lateral lobe segment) sampling strategies were used for the measurement (Figure 1). All largest-fit ROIs were manually positioned on the homogeneous liver parenchyma at the level of the right main portal vein, avoiding visible vessels, bile ducts and artifacts, with a mean size of 6.5 cm^2 (range, $3.2\text{--}13 \text{ cm}^2$). The first measurement of observer 1 and observer 2 was analyzed for inter-observer agreement. Observer 1 measured the parameters twice in a subset of 40 randomly selected patients (23 men and 17 women) from the study cohort to assess intra-observer agreement, and the interval between the data measurements was 7 days. As recently shown by Hong *et al.* (11), Four-ROI sampling strategies can achieve a close agreement with sampling all nine ROI hepatic segments. Average values of the four ROIs were used as a representative value of liver for each patient, and then the mean value of the two observers was used for statistical analysis.

Laboratory tests

All laboratory tests were performed before the liver biopsy, surgery, and MR examination. We selected common serum markers, including alanine aminotransferase (ALT), aspartate aminotransferase (AST), total bilirubin (TBIL), and platelet count.

Histopathologic evaluation

Forty-six patients with liver tumor underwent partial hepatectomy, and the surrounding hepatic parenchyma was sampled during liver resection. Fifty-three patients with CLDs underwent percutaneous US-guided liver biopsy in the right lobes. The interval between the biopsy or hepatectomy and MR imaging ranged from 1 to 6 days, with a mean of 3 days. The pathological samples were fixed with 10% formalin and routinely embedded in paraffin. The tissue slices were stained with hematoxylin-eosin, Masson trichrome, reticular fiber and Perl's Prussian blue staining. An experienced pathologist who was blinded to the clinical data and MR findings evaluated the slides.

According to the proportion of hepatocytes containing fat vesicles, liver steatosis was graded as follows (18): grade 0, less than 5.0%; grade 1, between 5.0% and 33.0%; grade 2, between 33.0% and 66.0%; and grade 3, more than 66.0%. Iron overload was classified from grade 0 to 4 based on visual assessment of iron granules with Prussian blue stain at different magnifications (19). Liver fibrosis stage and necroinflammatory activity were evaluated semiquantitatively according to the METAVIR scoring system (20). Fibrosis staging was categorized as follows: F0, no fibrosis; F1, portal fibrosis without septa; F2, portal fibrosis and few septa; F3, numerous septa without cirrhosis; F4, cirrhosis. The necroinflammatory activity was graded as follows: A0, none; A1, mild; A2, moderate; A3, severe.

Statistical analysis

Continuous variables were presented as means and standard deviations or medians and confidence intervals. Categorical variables were presented as numbers and percentages. Data distributions were tested for normality with Shapiro-wilk test. We test the interobserver agreement in a subset of 40 patients randomly chosen from the study cohort. Intra- and inter-observer agreement of Dixon parameters measurements were assessed by intraclass correlation coefficient (ICC). The difference of imaging parameters

between different histopathologic grading or staging were compared using analysis of variance (when data were normally distributed) or nonparametric Kruskal-Wallis test (when data were not normally distributed). In the case of statistical significance, multiple pairwise comparisons were performed using post hoc Tukey HSD test or post hoc Mann-Whitney test and the Bonferroni correction.

The relationship between different histopathologic and biochemical features (steatosis, iron overload, fibrosis stage, inflammation grade, ALT, AST, and TBIL) and 3D ME Dixon parameters was determined through nonparametric Spearman correlation coefficients. Multiple linear regression with stepwise selection of variable was performed to identify which histopathologic parameters correlated independently with Dixon parameters (MRI-PDFF and R2*). Receiver operating characteristics (ROC) analyses were used to evaluate the diagnostic performance of Dixon parameters for assessment of the liver steatosis or liver iron overload grading. The optimal cutoff values were chosen to maximize the sum of sensitivity and specificity, and the corresponding sensitivity, specificity, positive and negative predictive values were calculated. For all tests, a two-tailed P value of less than 0.05 was considered statistically significant. All statistical tests were performed using SPSS software (Version 18.0) and MedCalc (Version 13.1.2.0).

Results

Characteristics of patients

In the 99 patients, 46 hepatitis B patients underwent partial hepatectomy, including 41 patients with HCC, 3 patients with intrahepatic cholangiocarcinoma (ICC), and 2 patients with combined hepatocellular-cholangiocarcinoma (HCC-ICC). Other 53 patient with CLDs indicated for liver biopsy had the following causes: chronic hepatitis B (n=5, 9%), nonalcoholic fatty liver disease (n=14, 26%), alcoholic steatohepatitis (n=1, 2%), primary sclerotic cholangitis (n=8, 15%), autoimmune hepatitis (n=10, 19%), overlap syndrome of autoimmune CLD (n=5, 10%) and drug-induced hepatitis (n=10, 19%). MR examinations were performed before liver biopsy or partial hepatectomy.

Clinical, biochemical data and histopathologic findings are summarized in *Table 1*. Liver steatosis was observed in 40 (40.4%) of patients, and iron overload was present in 36 (36.4%) of patients. Moreover, 8 (8.1%) patients had both steatosis and iron overload. The mean percentage of histologic steatosis was 14.08%±21.26% (median, 3%;

range, 0–85%).

3D ME Dixon parameters measurements

Intra-observer agreement of MRI-PDFF and $R2^*$ was both excellent, and ICC was 0.993 (95% CI, 0.989–0.995) for

Table 1 Clinical and histological characteristics of the study population (n=99)

Characteristic	Value
Sex (male/female)	53/46
Age (years)	48.39±17 [23–77]
AST level (U/L)	148.7±607.83 [12–1,454]
ALT levels (U/L)	176.75±342.45 [8–1,883]
TBIL (mg/dL)	53.02±119.22 [6–324]
Platelet count ($10^9/L$)	156.46±260.22 [31–1,108]
Steatosis grade	
S0/S1/S2/S3/S4	59/22/17/1
Iron overload	
Grade 0/1/2/3	63/24/10/2
Fibrosis stage	
F0/F1/F2/F3/F4	8/23/16/21/31
Necroinflammatory activity	
A0/A1/A2/A3	2/30/40/27

Continuous data are expressed as means, with ranges in brackets. Categorical data are expressed as numbers of patients. ALT, alanine aminotransferase; AST, aspartate aminotransferase; TBIL, total bilirubin.

MRI-PDFF, and 0.983 (95% CI, 0.967–0.985) for $R2^*$. Inter-observer agreement of MRI-PDFF and $R2^*$ was excellent, and ICC was 0.977 (95% CI, 0.967–0.985) for MRI-PDFF, and 0.961 (95% CI, 0.943–0.974) for $R2^*$.

Mean MRI-PDFF in the liver was $7.27\% \pm 7.58\%$ (median 3.75%; range, 4.13–31.10%). MRI-PDFF differed significantly among no steatosis, mild steatosis, and moderate to severe steatosis groups ($P < 0.001$) (Figure 2A). Using post hoc analysis, significant differences existed in pairwise comparisons (all $P < 0.001$). Mean $R2^*$ in the liver was $54.01 \pm 16.15 S^{-1}$ (median, $49.72 S^{-1}$; range, 27.93–108.89 S^{-1}). A significant difference was observed among no iron overload (Grade 0), mild iron overload (Grade 1), and moderate to severe iron overload (Grade 2–3) ($P < 0.001$) (Figure 2B). Using post hoc analysis, significant differences existed in pairwise comparisons ($P = 0.000$ to 0.003).

Relationship between 3D ME Dixon parameter measurements and histologic findings

According to univariate analysis, a strong correlation was observed between MRI-PDFF and liver steatosis ($r = 0.858$, $P < 0.001$). Iron overload ($r = -0.219$, $P = 0.031$) and inflammation ($r = 0.304$, $P = 0.002$) had significant weak correlation with MRI-PDFF. $R2^*$ value was positively with both liver iron overload ($r = 0.743$, $P < 0.001$), fibrosis ($r = 0.366$, $P < 0.001$), and inflammation ($r = 0.211$, $P = 0.036$) (Table 2).

In the multiple regression analysis, liver steatosis was the only factor that independently influenced MRI-PDFF in this study and explained 80.3% of the variance in its values ($R^2 = 0.803$, $\beta = 0.896$, $P < 0.001$). However, liver iron overload

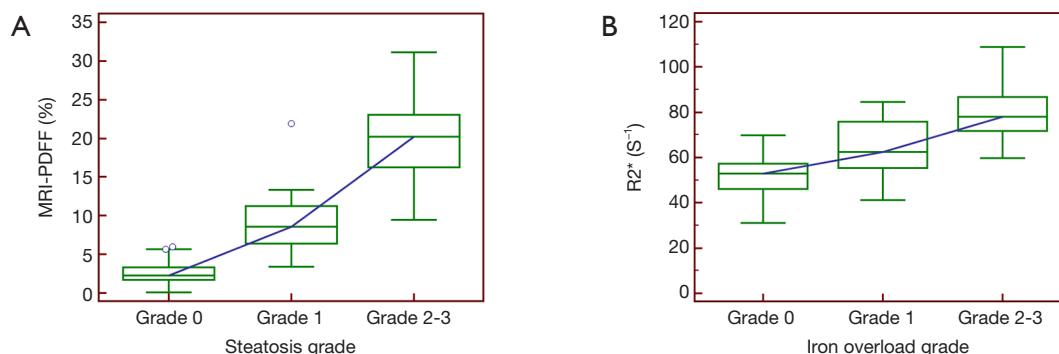


Figure 2 Box and whisker plot shows MR-PDFF (A) and $R2^*$ (B) is higher with progressively larger histological grade. Significant differences were found in all pairwise comparisons by using the Mann-Whitney test with Bonferroni correction (all $P < 0.005$). PDFF, proton density fat fraction.

Table 2 Effect of histopathological features on 3D ME Dixon parameters: univariate and multiple regression analyses

Variables	Univariate analysis		Multiple regression analysis		
	r	P	R2	β	P
MRI-PDFF					
Steatosis	0.858	<0.001	0.803	0.896	<0.001
Iron overload	-0.219	0.031	-	-	-
Fibrosis	-0.015	0.884	-	-	-
Inflammation	0.304	0.002	-	-	-
ALT level	0.046	0.53	-	-	-
AST level	-0.015	0.886	-	-	-
TBIL level	-0.001	0.994	-	-	-
R2* value					
Steatosis	-0.072	0.481	-	-	-
Iron overload	0.743	<0.001	0.647	0.767	<0.001
Fibrosis	0.366	<0.001	0.647	0.13	<0.001
Inflammation	0.211	0.036	-	-	-
ALT level	0.035	0.735	-	-	-
AST level	-0.013	0.898	-	-	-
TBIL level	0.035	0.734	-	-	-

PDFF, proton density fat fraction; ALT, alanine aminotransferase; AST, aspartate aminotransferase; TBIL, total bilirubin.

Table 3 Diagnostic performance of MRI-PDFF in assessment of liver steatosis

Statistic	Grade 0 versus 1–3	Grade 0–1 versus 2–3
AUC	0.989 (0.944–1.000)	0.986 (0.938–0.999)
P value	<0.0001	<0.0001
Cutoff value (%)	5.04	13.34
Sensitivity	95.0% (83.1–99.4%)	94.4% (72.7–99.9%)
Specificity	94.9% (85.9–98.9%)	98.8% (93.3–100%)

Numbers in parentheses are 95% confidence intervals. AUC, area under the ROC curve; PDFF, proton density fat fraction.

and fibrosis were the independent factors that contributed to R2* value [β=0.767, and 0.13 (P<0.001), respectively], and approximately 64.7% of the total variability in R2* values could be explained by two variables in this model (R²=0.647, P<0.001) (Table 2). To further subgroup analysis, a moderate positive correlation was found between R2* and fibrosis

Table 4 Diagnostic performance of R2* in assessment of liver iron overload

Statistic	Grade 0 versus 1–3	Grade 0–1 versus 2–3
AUC	0.815 (0.724–0.886)	0.876 (0.795–0.934)
P value	<0.0001	<0.0001
Cutoff value (S ⁻¹)	58.7	68.06
Sensitivity	75.0% (57.8–87.9%)	91.7% (61.5–99.8%)
Specificity	84.1% (72.7–92.1%)	89.7% (81.3–95.2%)

Numbers in parentheses are 95% confidence intervals. AUC, area under the ROC curve.

stage in patients without iron overload (r=0.542, P<0.001).

Diagnostic performance of 3D ME Dixon parameters

The AUC values, optimal cutoff values, and corresponding diagnostic performance for MRI-PDFF and R2* are shown in Tables 3,4, respectively. The cut-off value of MRI-PDFF measurement was 5.04% (AUC =0.989; 95% CI, 0.944–1.000) to identify mild grade steatosis or higher (≥ grade 1), and 13.34% (AUC =0.986; 95% CI, 0.938–0.999) to determine moderate grade steatosis or higher (≥ grade 2) (Table 3, Figure 3). The cut-off value of R2* was 58.7 S⁻¹ (AUC =0.815; 95% CI, 0.724–0.886) to identify mild or higher iron overload (≥ grade 1), and 68.06 S⁻¹ (AUC =0.876; 95% CI, 0.795–0.934) to identify moderate or higher iron overload (≥ grade 2) (Table 4, Figure 4).

Discussion

In the present study, we evaluated the feasibility of 3D ME Dixon sequence for simultaneous assessment of liver steatosis and liver iron overload in the presence of CLDs, specifically in liver fibrosis and inflammation. Our study demonstrated that liver steatosis is independently associated with MRI-PDFF derived from 3D ME Dixon (β=0.896, P<0.001), whereas liver iron overload and liver fibrosis were independent factors that contributed to R2* value (β=0.767 and 0.13, respectively; P<0.001). The AUC showed that 3D ME Dixon had high accuracy for simultaneous diagnosis of liver steatosis and iron overload in patients with CLDs, with good to excellent diagnostic performance (AUC ranging from 0.815 to 0.989). These findings suggest that 3D ME Dixon has an important clinical significance for the management of patients with CLDs.

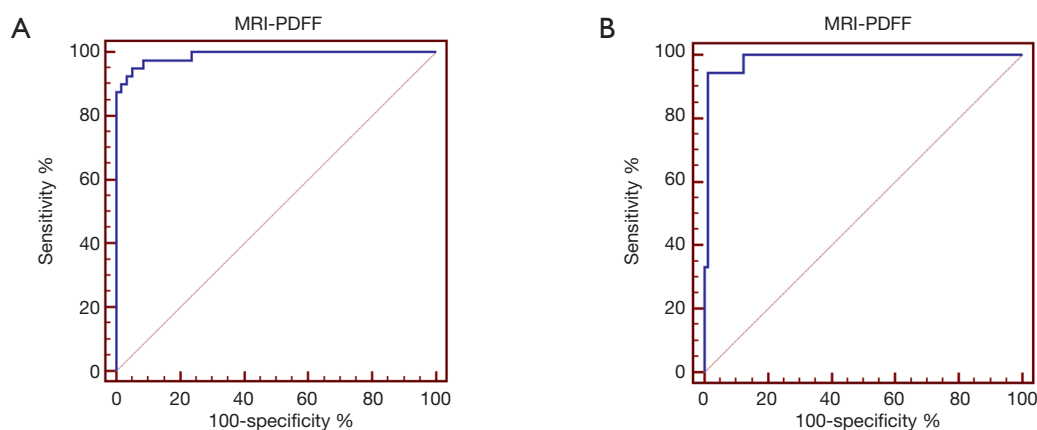


Figure 3 Receiver operating characteristic curve (ROC) of MRI-PDFF for the identification of mild grade steatosis or higher (\geq grade 1) (A) and moderate grade or higher (\geq grade 2) (B). PDFF, proton density fat fraction.

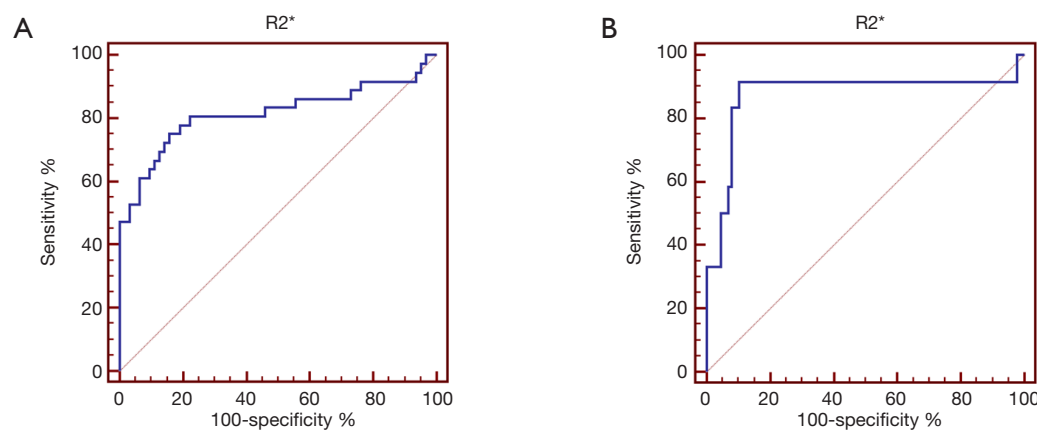


Figure 4 Receiver operating characteristic curve (ROC) of $R2^*$ for the identification of mild grade iron overload or higher (\geq grade 1) (A) and moderate grade or higher (\geq grade 2) (B).

A recent meta-analysis of Yokoo *et al.* (10) suggested excellent linearity, negligible bias, and high precision of MRI-PDFF across different field strengths, imager manufacturers, and reconstruction methods. We found that MRI-PDFF strongly correlated with the steatosis grade, which is consistent with previous studies (21–26). Furthermore, our results demonstrated that potential histopathological confounding factors (e.g., liver fibrosis, inflammation, and iron deposition) did not significantly influence MRI-PDFF. Our results were consistent with prior studies, which supports that liver fibrosis or inflammation has no significant effect on MRI-PDFF measurement (21,25,27,28). Although Idilman *et al.* (22) shown that liver fibrosis reduced the correlation between MRI-PDFF and liver biopsy-determined steatosis, they did

not further perform multivariate analysis. Also, previous studies have shown that MRI-PDFF can accurately grade liver steatosis (13,14,21,29). Similarly, our data demonstrated that MRI-PDFF had an excellent diagnostic performance for grading liver steatosis, with AUC of 0.989 for the diagnosis of grade 1 or higher steatosis and 0.986 for grade 2 or higher steatosis. These findings confirmed that MRI-PDFF could be used as a noninvasive imaging biomarker for liver steatosis with a wide spectrum of CLDs.

Several technical factors must be considered for more accurate estimation of $R2^*$, such as spectral modeling of fat, noise floor effect, fitting model, and the number of echoes. However, there is substantial controversy as to whether an accurate signal model should combine or separate the $R2^*$ values for fat and water (30). Two- $R2^*$ fitting model

for separate water and fat $R2^*$ leads to algorithm instability and noise amplification (31). In general, the single $R2^*$ approach that assumed the same $T2^*$ relaxation of water and fat is sufficient and accurate (30,31). Although more echoes improve $T2^*$ estimation and correction, Yu *et al.* (32) found that 6-echo acquisitions achieve a good balance of short scan time and improved $T2^*$ estimation. In our study, a single effective $R2^*$ value of the water-fat mixture was generated by acquiring 6 echoes with non-linear fitting. The positive correlation was observed between $R2^*$ values and iron grades in our study ($r=0.743$, $P<0.001$), which is similar to previous studies (25,33,34). Also, our results indicated that $R2^*$ values were independently influenced by both liver iron overload and liver fibrosis ($P<0.001$).

Moreover, a moderate correlation was observed between $R2^*$ value and liver fibrosis in the subset of patients without iron overload ($r=0.542$, $P<0.001$). Based on our data, we speculate that increased $R2^*$ could reflect liver fibrosis in the absence of iron overload. Likewise, previous studies suggested that $R2^*$ values may also be affected by factors such as fibrosis (35). In contrary to our study, França *et al.* (25) reported that $R2^*$ values were not influenced by fibrosis. The possible explanations for this discrepancy were different included population and statistical method. Theoretically, the excess accumulation of extracellular matrix and progressive fibrosis lead to heterogeneity of liver background, which could lead to $T2^*$ decay and signal loss. This may be possible to explain why $R2^*$ value was correlated with liver fibrosis. However, this hypothesis needs to be investigated in future studies.

Currently, MRS is considered the most accurate noninvasive approach for liver fat quantification. Limitations to the routine use of MRS in liver fat quantification include the complexity of spectral analysis and sampling error due to acquisition in only a small region of the liver. In recent years, it has been shown that multi-echo $T2$ corrected single voxel spectroscopy (HISTO) can be used for reliable liver fat quantification within single breath-hold acquisition (36-38). Several studies (10,28,39-41) have validated that the excellent correlation and agreement between MRS- and MRI-PDF. Besides, HISTO sequence also allows simultaneous estimation of liver iron deposition using $R2$ value. Although promising, most studies focused on PDF derived from HISTO sequence rather than $R2$ value. Further studies are warranted to determine the diagnostic performance of HISTO for simultaneous quantification of liver fat and iron deposition. Additionally, HISTO also acquires a single anatomical location and encounters

sampling variability. Due to spatial heterogeneity of hepatic fat and iron deposition (5), HISTO sequence is not an ideal tool for whole-liver overload evaluation. In contrast, the main advantage of 3D ME Dixon enables whole-liver coverage in a single breath-hold acquisition and is early incorporated into the routine liver examination.

This study has several limitations. First, patients were not distributed equally among different histopathological grades, particularly in the small number of patients with a severe grade, which may introduce statistical bias. Further validation study including a larger number of patients with various degrees of liver steatosis and iron overload is warranted. Second, we did not evaluate the influence of ROI sampling strategies on measurement reproducibility of 3D ME Dixon parameters. Campo *et al.* (42) showed that the reproducibility and repeatability of liver PDF and $R2^*$ measurements improve as the liver sampling area increases through the use of ROIs that are large in both number and size. Sofue *et al.* (43) showed that MRI-PDF and $R2^*$ were repeatable between examinations. Hong *et al.* (11) demonstrated that four-ROI sampling strategies with two ROIs in the left and right lobes achieve a close agreement with nine-ROI PDF. In this study, we used the average value of four ROIs as a representative of the whole liver. Third, liver specimens were only analyzed by semiquantitative histological assessment rather than the biochemical determination of liver iron concentration. A further validation study is needed to confirm the results.

In summary, our findings indicate that 3D ME Dixon is an accurate, non-invasive technique for simultaneous assessment of liver steatosis and iron overload in patients with CLDs, especially for quantification of liver steatosis. MRI-PDF derived from 3D ME Dixon may be used as an alternative, surrogate imaging biomarker to histopathologic estimation for detection and grading of liver steatosis in patients with CLDs. However, $R2^*$ value may be affected by the liver fibrosis in the setting of CLDs with the absence of iron overload.

Acknowledgments

Funding: This study was funded by the National Natural Science Foundation of China (Grant Number 81471658).

Footnote

Conflicts of Interest: The authors have no conflicts of interest to declare.

Ethical Statement: This retrospective study was approved by the Institutional Review Board (IRB), and informed consent was waived.

References

- Rinella M, Charlton M. The globalization of nonalcoholic fatty liver disease: Prevalence and impact on world health. *Hepatology* 2016;64:19-22.
- Reeder SB, Cruite I, Hamilton G, Sirlin CB. Quantitative assessment of liver fat with magnetic resonance imaging and spectroscopy. *J Magn Reson Imaging* 2011;34:729-49.
- Hernando D, Levin YS, Sirlin CB, Reeder SB. Quantification of liver iron with MRI: state of the art and remaining challenges. *J Magn Reson Imaging* 2014;40:1003-21.
- Sharma P, Altbach M, Galons JP, Kalb B, Martin DR. Measurement of liver fat fraction and iron with MRI and MR spectroscopy techniques. *Diagn Interv Radiol* 2014;20:17-26.
- Yokoo T, Browning JD. Fat and iron quantification in the liver: past, present, and future. *Top Magn Reson Imaging* 2014;23:73-94.
- Powell EE, Ali A, Clouston AD, et al. Steatosis is a cofactor in liver injury in hemochromatosis. *Gastroenterology* 2005;129:1937-43.
- Tapper EB, Lok AS. Use of Liver Imaging and Biopsy in Clinical Practice. *N Engl J Med* 2017;377:756-68.
- Cassidy FH, Yokoo T, Aganovic L, et al. Fatty liver disease: MR imaging techniques for the detection and quantification of liver steatosis. *Radiographics* 2009;29:231-60.
- Sirlin CB, Reeder SB. Magnetic resonance imaging quantification of liver iron. *Magn Reson Imaging Clin N Am* 2010;18:359-81.
- Yokoo T, Serai SD, Pirasteh A, et al. Linearity, Bias, and Precision of Hepatic Proton Density Fat Fraction Measurements by Using MR Imaging: A Meta-Analysis. *Radiology* 2018;286:486-98.
- Hong CW, Wolfson T, Sy EZ, Schlein AN, Hooker JC, Fazeli Dehkordy S, Hamilton G, Reeder SB, Loomba R, Sirlin CB. Optimization of region-of-interest sampling strategies for hepatic MRI proton density fat fraction quantification. *J Magn Reson Imaging* 2018;47:988-94.
- Caussy C, Reeder SB, Sirlin CB, Loomba R. Noninvasive, Quantitative Assessment of Liver Fat by MRI-PDFF as an Endpoint in NASH Trials. *Hepatology* 2018;68:763-72.
- Middleton MS, Heba ER, Hooker CA, Bashir MR, Fowler KJ, Sandrasegaran K, Brunt EM, Kleiner DE, Doo E, Van Natta ML, Lavine JE, Neuschwander-Tetri BA, Sanyal A, Loomba R, Sirlin CB; NASH Clinical Research Network. Agreement Between Magnetic Resonance Imaging Proton Density Fat Fraction Measurements and Pathologist-Assigned Steatosis Grades of Liver Biopsies From Adults With Nonalcoholic Steatohepatitis. *Gastroenterology* 2017;153:753-61.
- Middleton MS, Van Natta ML, Heba ER, et al. Diagnostic accuracy of magnetic resonance imaging hepatic proton density fat fraction in pediatric nonalcoholic fatty liver disease. *Hepatology* 2018;67:858-72.
- Artz NS, Haufe WM, Hooker CA, et al. Reproducibility of MR-based liver fat quantification across field strength: Same-day comparison between 1.5T and 3T in obese subjects. *J Magn Reson Imaging* 2015;42:811-7.
- Kang GH, Cruite I, Shiehorteza M, et al. Reproducibility of MRI-determined proton density fat fraction across two different MR scanner platforms. *J Magn Reson Imaging* 2011;34:928-34.
- Petitclerc L, Sebastiani G, Gilbert G, Cloutier G, Tang A. Liver fibrosis: Review of current imaging and MRI quantification techniques. *J Magn Reson Imaging* 2017;45:1276-95.
- Yokoo T, Shiehorteza M, Hamilton G, Wolfson T, Schroeder ME, Middleton MS, Bydder M, Gamst AC, Kono Y, Kuo A, Patton HM, Horgan S, Lavine JE, Schwimmer JB, Sirlin CB. Estimation of hepatic proton-density fat fraction by using MR imaging at 3.0 T. *Radiology* 2011;258:749-59.
- Deugnier Y, Turlin B. Pathology of hepatic iron overload. *World J Gastroenterol* 2007;13:4755-60.
- Bedossa P, Poynard T. An algorithm for the grading of activity in chronic hepatitis C. The METAVIR Cooperative Study Group. *Hepatology* 1996;24:289-93.
- Tang A, Tan J, Sun M, Hamilton G, Bydder M, Wolfson T, Gamst AC, Middleton M, Brunt EM, Loomba R, Lavine JE, Schwimmer JB, Sirlin CB. Nonalcoholic fatty liver disease: MR imaging of liver proton density fat fraction to assess hepatic steatosis. *Radiology* 2013;267:422-31.
- Idilman IS, Aniktar H, Idilman R, Kabacam G, Savas B, Elhan A, Celik A, Bahar K, Karcaaltincaba M. Hepatic steatosis: quantification by proton density fat fraction with MR imaging versus liver biopsy. *Radiology* 2013;267:767-75.
- Joe E, Lee JM, Kim KW, Lee KB, Kim SJ, Baek JH, Shin CI, Suh KS, Yi NJ, Han JK, Choi BI. Quantification of hepatic macrosteatosis in living, related liver donors using

- T1-independent, T2*-corrected chemical shift MRI. *J Magn Reson Imaging* 2012;36:1124-30.
24. Kang BK, Kim M, Song SY, Jun DW, Jang K. Feasibility of modified Dixon MRI techniques for hepatic fat quantification in hepatic disorders: validation with MRS and histology. *Br J Radiol* 2018;91:20170378.
 25. França M, Alberich-Bayarri Á, Martí-Bonmatí L, Oliveira P, Costa FE, Porto G, Vizcaíno JR, Gonzalez JS, Ribeiro E, Oliveira J, Pessequeiro Miranda H. Accurate simultaneous quantification of liver steatosis and iron overload in diffuse liver diseases with MRI. *Abdom Radiol (NY)* 2017;42:1434-43.
 26. Kühn JP, Hernando D, Muñoz del Rio A, Evert M, Kannengiesser S, Völzke H, Mensel B, Puls R, Hosten N, Reeder SB. Effect of multipeak spectral modeling of fat for liver iron and fat quantification: correlation of biopsy with MR imaging results. *Radiology* 2012;265:133-42.
 27. Parente DB, Rodrigues RS, Paiva FF, Oliveira Neto JA, Machado-Silva L, Lanzoni V, Campos CF, Eiras-Araujo AL, do Brasil PE, Garteiser P, Gomes MB, de Mello Perez R. Is MR spectroscopy really the best MR-based method for the evaluation of fatty liver in diabetic patients in clinical practice? *PLoS One* 2014;9:e112574.
 28. Kang BK, Yu ES, Lee SS, Lee Y, Kim N, Sirlin CB, Cho EY, Yeom SK, Byun JH, Park SH, Lee MG. Hepatic fat quantification: a prospective comparison of magnetic resonance spectroscopy and analysis methods for chemical-shift gradient echo magnetic resonance imaging with histologic assessment as the reference standard. *Invest Radiol* 2012;47:368-75.
 29. Tang A, Desai A, Hamilton G, Wolfson T, Gamst A, Lam J, Clark L, Hooker J, Chavez T, Ang BD, Middleton MS, Peterson M, Loomba R, Sirlin CB. Accuracy of MR imaging-estimated proton density fat fraction for classification of dichotomized histologic steatosis grades in nonalcoholic fatty liver disease. *Radiology* 2015;274:416-25.
 30. Zhong X, Nickel MD, Kannengiesser SA, Dale BM, Kiefer B, Bashir MR. Liver fat quantification using a multi-step adaptive fitting approach with multi-echo GRE imaging. *Magn Reson Med* 2014;72:1353-65.
 31. Horng DE, Hernando D, Reeder SB. Quantification of liver fat in the presence of iron overload. *J Magn Reson Imaging* 2017;45:428-39.
 32. Yu H, McKenzie CA, Shimakawa A, Vu AT, Brau AC, Beatty PJ, Pineda AR, Brittain JH, Reeder SB. Multiecho reconstruction for simultaneous water-fat decomposition and T2* estimation. *J Magn Reson Imaging* 2007;26:1153-61.
 33. Banerjee R, Pavlides M, Tunnicliffe EM, Piechnik SK, Sarania N, Philips R, Collier JD, Booth JC, Schneider JE, Wang LM, Delaney DW, Fleming KA, Robson MD, Barnes E, Neubauer S. Multiparametric magnetic resonance for the non-invasive diagnosis of liver disease. *J Hepatol* 2014;60:69-77.
 34. Chandarana H, Lim RP, Jensen JH, Hajdu CH, Losada M, Babb JS, Huffman S, Taouli B. Hepatic iron deposition in patients with liver disease: preliminary experience with breath-hold multiecho T2*-weighted sequence. *AJR Am J Roentgenol* 2009;193:1261-7.
 35. Wood JC. Magnetic resonance imaging measurement of iron overload. *Curr Opin Hematol* 2007;14:183-90.
 36. Pineda N, Sharma P, Xu Q, Hu X, Vos M, Martin DR. Measurement of hepatic lipid: high-speed T2-corrected multiecho acquisition at 1H MR spectroscopy--a rapid and accurate technique. *Radiology* 2009;252:568-76.
 37. Hayashi N, Miyati T, Minami T, Takeshita Y, Ryu Y, Matsuda T, Ohno N, Hamaguchi T, Kato K, Takamura T, Matsui O. Quantitative analysis of hepatic fat fraction by single-breath-holding MR spectroscopy with T(2) correction: phantom and clinical study with histologic assessment. *Radiol Phys Technol* 2013;6:219-25.
 38. Lee SS, Lee Y, Kim N, Kim SW, Byun JH, Park SH, Lee MG, Ha HK. Hepatic fat quantification using chemical shift MR imaging and MR spectroscopy in the presence of hepatic iron deposition: validation in phantoms and in patients with chronic liver disease. *J Magn Reson Imaging* 2011;33:1390-8.
 39. Meisamy S, Hines CD, Hamilton G, Sirlin CB, McKenzie CA, Yu H, Brittain JH, Reeder SB. Quantification of hepatic steatosis with T1-independent, T2-corrected MR imaging with spectral modeling of fat: blinded comparison with MR spectroscopy. *Radiology* 2011;258:767-75.
 40. Achmad E, Yokoo T, Hamilton G, Heba ER, Hooker JC, Changchien C, Schroeder M, Wolfson T, Gamst A, Schwimmer JB, Lavine JE, Sirlin CB, Middleton MS. Feasibility of and agreement between MR imaging and spectroscopic estimation of hepatic proton density fat fraction in children with known or suspected nonalcoholic fatty liver disease. *Abdom Imaging* 2015;40:3084-90.
 41. Bashir MR, Zhong X, Nickel MD, Fananapazir G, Kannengiesser SA, Kiefer B, Dale BM. Quantification of hepatic steatosis with a multistep adaptive fitting MRI approach: prospective validation against MR spectroscopy. *AJR Am J Roentgenol* 2015;204:297-306.
 42. Campo CA, Hernando D, Schubert T, Bookwalter CA,

- Pay A, Reeder SB. Standardized Approach for ROI-Based Measurements of Proton Density Fat Fraction and R2* in the Liver. *AJR Am J Roentgenol* 2017;209:592-603.
43. Sofue K, Mileto A, Dale BM, Zhong X, Bashir MR.

Interexamination repeatability and spatial heterogeneity of liver iron and fat quantification using MRI-based multistep adaptive fitting algorithm. *J Magn Reson Imaging* 2015;42:1281-90.

Cite this article as: Hu F, Yang R, Huang Z, Wang M, Yuan F, Xia C, Wei Y, Song B. 3D Multi-Echo Dixon technique for simultaneous assessment of liver steatosis and iron overload in patients with chronic liver diseases: a feasibility study. *Quant Imaging Med Surg* 2019;9(6):1014-1024. doi: 10.21037/qims.2019.05.20